CHAPTER 10

COLLISIONLESS SHOCK WAVES

A shock may be defined as a layer of rapid change propagating through the plasma. In its rest frame, the shock is approximately invariable in time and is marked by a rapid transition of parameters from the medium ahead (also called *upstream*) to the medium behind the shock (*downstream*). A simple example of a shock occurs when a plane piston moves at high velocity into a homogeneous plasma at rest. A shock develops ahead of the piston between the piled-up plasma and the undisturbed plasma. The shock propagates at a velocity similar to or higher velocity than that of the piston. Another example is a wave (or a pulse) with an amplitude so high that the wave velocity of the crest is faster than the velocity of the dip. Small disturbances thus travel faster on the wave crest, overtake it and add in front of it. The wave profile steepens in the front of the wave crest and develops into a shock (like an ocean wave approaching a sloping beach steepens and finally breaks).

A characteristic property of shocks is the dissipation of energy and increasing entropy as it moves through the plasma. The region of energy dissipation, called the *shock front*, is generally extremely thin compared to the lateral extension. It is often approximated by a surface.

The shock structures emphasized in this chapter are those that occur in low-density, fully ionized plasmas – such as coronae – where the collisional mean free path is much longer than the width of the structure. Momentum and energy of a disturbance are transferred across the shock by electric and magnetic fields, and waves. Such collisionless shock waves are produced by numerous violent processes in coronae, and in interplanetary and interstellar space. The eruptions of a coronal prominence or, on a smaller scale, of a surge or a spicule, are likely to generate a disturbance that propagates ahead and into the corona. Shocks are predicted in the outflows expelled by the reconnection process. Solar flares can produce shocks reverberating throughout the heliosphere. Strong collisionless shocks are conspicuous by associated particles, some of them – as in supernova remnants – accelerated to highly relativistic energies. Most of our knowledge on the physics of collisionless shocks, however, comes from much closer to home: spacecraft have gathered a rich collection of data at the Earth's bow shock and in the interplanetary medium over the past three decades.

In the logical sequence from simple to complex plasma phenomena, non-linear waves and shocks claim the final position. The field of collisionless shocks is too vast to be covered adequately in this limited space. We give here some fundamentals and concentrate on the astrophysically most interesting aspects of particle acceleration and heating.

Plasma Astrophysics
A. O. Benz, Kluwer Academic publishers
2002

10.1. Elementary Concepts

The basic equations for shocks are the same as for any plasma phenomenon: the Boltzmann equation (1.4.11) – or the Vlasov equation (5.2.1) for the collisionless case – and Maxwell's equations (1.4.2) – (1.4.5). As in Chapter 3 on linear waves, conservation of mass, momentum, and energy densities can greatly facilitate the treatment of shocks if the velocity distribution of the particles is such that the conserved moments can be analytically computed. Here, the theme is not the conservation of an equilibrium state being slightly disturbed by a wave, but the focus is on conservation laws in the large-amplitude transition of plasma parameters at the shock.

10.1.1. Types of Shocks

There is an impressive variety of shocks in nature. In the classical *hydrodynamic* shock, the disturbance is propagated by collisions. A conducting gas with a magnetic field and (collision-dominated) Maxwellian particle distributions – described by the *magnetohydrodynamic* (MHD) equations – has three types of shock solutions in analogy with the fast, intermediate (Alfvénic), and slow MHD modes of linear waves. Correspondingly, the MHD shock description classifies fast-mode, intermediate-mode, and slow-mode shocks. They are usually abbreviated to *fast*, *intermediate*, and *slow shock*. Figure 10.1 depicts the three possibilities of the magnetic field orientation behind a shock moving at an oblique angle to the magnetic field of the plasma ahead.

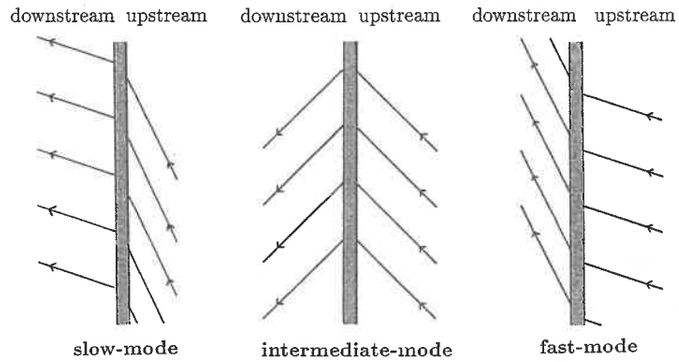

Fig. 10.1. The changes in magnetic field direction (arrow) from ahead (upstream) to behind (downstream) an MHD shock are characteristic for its type.

In all shocks, the component of the magnetic field normal to the shock front is continuous across the shock. This assures continuity of field lines. The component of the magnetic field tangential to the shock front increases across fast shocks, decreases across slow shocks, and remains equal for intermediate shocks.

MHD shocks travel faster than the linear MHD modes. In the limit where the compression ratio of downstream to upstream density approaches unity, the fast, intermediate, and slow shocks reduce to the corresponding linear waves and propagate at their phase velocities (Fig. 3.1). Similar to the linear wave modes, only one type of MHD shock can propagate perpendicular to the magnetic field, namely the fast shock.

The thickness of an MHD shock is limited by the distance to dissipate the energy. We estimate it in two thought experiments. (*i*) In a non-magnetic situation (such as an acoustic (slow) shock moving parallel to the magnetic field ahead), the scale of energy dissipation is roughly the mean free path of thermal particles. Physically, this is the approximate distance the plasma behind the shock can influence the plasma ahead and *vice versa*. For an interplanetary density of $n_e \approx 10$ cm^{-3} and a temperature of $T \approx 10^5$ K, the non-magnetic shock thickness would be more than an astronomical unit. It is reduced by a factor of $\cos\theta$, if there is an angle θ between shock propagation and upstream magnetic field. Even that is many orders of magnitude longer than is actually observed.

(*ii*) Another form of energy dissipation is Ohmic heating due to finite conductivity. It may be relevant for shock propagation nearly perpendicular to the magnetic field (to be called *quasi-perpendicular* shocks). If it dominates, the shock thickness Δx can be estimated in the following way. The heating rate is

$$\frac{\partial \mathcal{E}}{\partial t} = \frac{J^2}{\sigma} \quad . \tag{10.1.1}$$

The current density may be approximated from Ampère's law and the magnetic fields ahead and behind the shock. Typical coronal values suggest an incredible shock thickness of some 10^{-4} cm (Exercise 10.1). This is smaller than important plasma length-scales, such as the ion gyroradius or the Debye length, and cannot be realistic either.

The thought experiments demonstrate that a description using Coulomb collisions is generally inadequate for the physics within the coronal shock layer. Kinetic plasma processes, and in particular collisionless waves, cause faster interactions between the upstream and downstream plasmas. This reduces effectively the mean free path and increases the heating rate (10.1.1). If the dominant dissipation mechanism is known, an order-of-magnitude estimate of the shock thickness may be obtained by equating energy input and dissipation rate in the rest frame of the shock.

The major variety of collisionless shock fronts may be called *turbulent*. They correspond to non-linear structures for which no single wave mode solution (collisional or collisionless) exists. Collisionless waves are driven by small-scale processes, such as unstable electric currents and beams. The interaction of the wave turbulence with particles simulates collisions. In effect, this causes an *MHD-like* shock phenomenon, where the width of the turbulent layer takes the role of the mean free path. It is therefore not surprising that MHD considerations often lead to quantitatively correct results by using some anomalous conductivity. In many coronal shocks, the electron and ion temperatures do not equilibrate within the shock, or the stresses between the media ahead and behind the shock may be transmitted entirely by non-thermal, energetic particles. Such cases can obviously not be approximated by MHD.

The different mobility of electrons and ions being compressed creates charge separations and electric fields. The electric potential of collisionless shocks can reflect ions approaching the front from ahead. Quasi-perpendicular shocks reflect ions at an appreciable number if the Alfvénic Mach number, $M_A := V_1/c_A$, exceeds a threshold (between about 1.1 and 2.2, depending on the upstream plasma parameters). V_1 is the shock velocity relative to the upstream medium. Such strong shocks are called *supercritical*. Their observational characteristic are ion streams in the region ahead of the shock causing intense low-frequency electromagnetic turbulence in a region called the *foot* of the shock (Fig. 10.3). The global shock structure changes at the threshold to supercritical behavior. In subcritical shocks, the energy is mainly dissipated by resistivity and most of the heating goes into electrons. Heating of both ions and electrons takes place in supercritical shocks as the wave profile breaks (i.e. ion reflection sets in) and other dissipation mechanisms, such as viscosity appear.

A further distinction of shocks is frequently made according to their driving agent. The extreme models are called *blast wave* and *piston-driven* shocks. The *blast wave* limit considers an impulsive deposition of mass, energy and momentum that is short compared to the propagation time. The input is an explosion, whose effects then propagate through the corona or interplanetary medium as a shock front. After the explosion, the flow at the site of explosion is soon exhausted and does not propagate to the point of observation. The observer only sees a disturbance passing by. In the *driven shock*, the hot material continues to be ejected from the source and follows the shock front. This case resembles the flows in a classic laboratory device called shock-tube, where a piston is driven into a gas. Astrophysical examples of pistons include destabilized magnetic loops or eruptive filaments, flare material, and supernova ejecta. Observations of the kinetic energy flux following immediately the passage of a shock front can distinguish the two types. At a given point of observation, the energy flux decreases with time behind blast waves; for driven shocks it rises. In interplanetary space, where shocks and energy flux can be observed, intermediate cases have also been reported.

In summary, shocks can be classified according to:

(1) particle velocity distribution: MHD or collisionless;

(2) angle between shock-normal and upstream magnetic field: quasi-perpendicular or quasi-transverse;

(3) ion acceleration: subcritical or supercritical;

(4) driving agent: blast wave or piston driven.

10.1.2. CONSERVATION EQUATIONS (MHD SHOCKS)

Consider a shock in its rest frame (Fig. 10.2). The plasma moving into the shock from upstream (right) leaves the shock layer downstream (left) at a different, smaller velocity. In equilibrium and in absence of sources and sinks, the inflowing mass, momentum, and energy must equal the outflowing values. It is instructive to further simplify the mathematics by assuming the MHD approximations (Section 3.1.3), implying that the velocity distributions ahead and behind the shock are Maxwellian and $T_e = T_i$. We shall show in this section how the three conservation equations then determine the downstream state entirely in terms of the shock velocity and the conditions ahead.

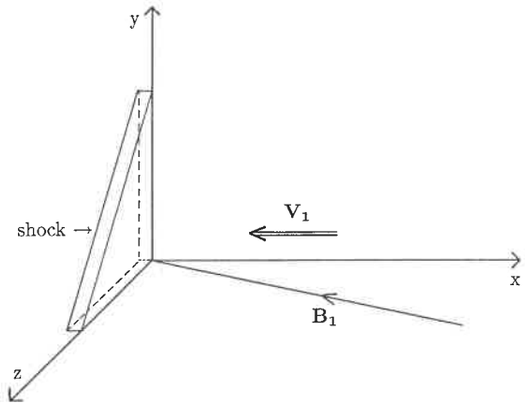

Fig. 10.2. A *normal incidence* frame of reference can be defined, in which the shock is at rest, the upstream velocity is normal ($V_{x1} = V_1$), and the magnetic field is in the (x, z)-plane (implying $B_{y1} = 0$ ahead of the shock).

Let the shock be stationary and homogeneous in the y and z directions of the coordinate system depicted by Figure 10.2. The normal incidence frame is one of the rest frames of the shock, moving along the front such that the inflow is normal to the front. It will furthermore be assumed that the mean velocities of the species are equal and that there is only one ion species, having a density $n_i = n_e$.

The MHD equation of continuity (3.1.40) is integrated in the x-direction from an arbitrary point 1 sufficiently far in the upstream medium through the shock to a point 2 downstream. The result, by partial integration, is

$$\rho_1 \, V_1 = \rho_2 \, V_{x2} \quad , \tag{10.1.2}$$

where $V_1 = V_{x1}$ is the shock speed. The equation expresses that the inflowing mass per unit area equals the outflow. An equation like (10.1.2) is called a *jump condition*. Since the regions ahead and behind the shock are assumed to be homogeneous, the subscripts 1 and 2 refer to the general conditions before and after the

shock. In a compression shock $\rho_2 > \rho_1$, thus $V_1 > V_{x2}$, and the incoming plasma is decelerated at the shock. The opposite would not be invariable: an expansion shock flattens as it propagates and finally disappears. It is not of interest here.

The conservation of momentum is described by the vector equation (3.1.50). Integrating the x-component over the x-direction, one derives again by partial integration

$$\rho_1 V_1^2 + p_1 + \frac{B_{z1}^2}{8\pi} \;=\; \rho_2 V_{x2}^2 + p_2 + \frac{B_{z2}^2}{8\pi} \quad . \tag{10.1.3}$$

The equation expresses pressure balance between the upstream and downstream plasmas. Note how the incoming energy is converted into heat and magnetic energy.

It has been used in Equation (10.1.3) that Ampère's equation requires $B_{y2} = 0$, and that the conservation of the y-component of momentum density results in $V_{y2} = 0$. The conservation of the z-component of momentum yields

$$\frac{B_{x1} B_{z1}}{4\pi} \;=\; \frac{B_{x2} B_{z2}}{4\pi} - \rho_2 V_{x2} V_{z2} \quad . \tag{10.1.4}$$

Energy conservation requires that the energy flow through the shock is constant. The flow is composed of kinetic energy, $\sum_\alpha \frac{1}{2} \int m_\alpha v^2 \mathbf{v} f_\alpha(v) d^3v$, and electromagnetic energy, $\mathbf{E} \times \mathbf{B} c/(4\pi)$. The conservation of the x-component requires

$$[5p_1 + \rho_1 V_1^2 + \frac{B_{z1}^2}{2\pi}] V_1 = [5p_2 + \rho_2 (V_{x2}^2 + V_{z2}^2) + \frac{B_{z2}^2}{2\pi}] V_{x2} - \frac{B_{x2} B_{z2}}{2\pi} V_{z2} \quad . \tag{10.1.5}$$

From the absence of magnetic monopoles ($\nabla \cdot \mathbf{B} = 0$) follows

$$B_{x1} = B_{x2} =: B_x \quad , \tag{10.1.6}$$

and from Faraday's law (using $\nabla \times \mathbf{E} = 0$) combined with $\mathbf{E} = -(\mathbf{V} \times \mathbf{B})/c$ one derives

$$V_1 B_{z1} \;=\; V_{x2} B_{z2} - V_{z2} B_x \quad . \tag{10.1.7}$$

Equations (10.1.2) – (10.1.7) relate the downstream parameters to the upstream state. They are generally called *Rankine-Hugoniot relations*. There is a general solution for each downstream MHD parameter in terms of upstream values. Since it is rather intricate and not instructive, we shall consider here three special cases.

If the shock speed is *extremely high*, the upstream energy density is dominated by the kinetic energy. Neglecting upstream magnetic and thermal energy density in Equation (10.1.3), the Rankine-Hugoniot relations reduce to

$$\frac{\mathbf{V}_{x2}}{\mathbf{V}_1} = \frac{\rho_1}{\rho_2} \approx \frac{1}{4} \tag{10.1.8}$$

and

$$p_2 \approx 3 \rho_2 V_{x2}^2 \tag{10.1.9}$$

(Exercise 10.2). Surprisingly, Equation (10.1.8) states a maximum compression ratio for strong shocks. Equation (10.1.9) expresses that the fraction of initial energy converted into thermal energy is 9/16 and is independent of the shock velocity. This heating is independent of the processes taking place in the shock layer as long as they yield Maxwellians and $T_e = T_i$. Heating is one of the prime reasons for interest in shock waves, both in the laboratory and in the universe, as it provides a controlled means of producing high-temperature plasmas.

For *perpendicular* fast-mode shocks ($B_{x1} = B_{x2} = 0$), the Rankine-Hugoniot relations simplify to

$$\frac{\mathbf{V}_{x2}}{\mathbf{V}_1} = \frac{n_1}{n_2} = \frac{B_{z1}}{B_{z2}} = \frac{1}{8}\left[1 + \frac{5p_1}{\rho_1 V_1^2} + \frac{5B_{z1}^2}{8\pi\rho_1 V_1^2}\right] + \frac{1}{8}\left[\left(1 + \frac{5p_1}{\rho_1 V_1^2} + \frac{5B_{z1}^2}{8\pi\rho_1 V_1^2}\right)^2 + \frac{2B_{z1}^2}{\pi\rho_1 V_1^2}\right]^{1/2} . \quad (10.1.10)$$

Equation (10.1.4) requires that $V_{z2} = 0$. A compression shock only exists if $V_{x2}/V_1 < 1$, thus from Equation (10.1.10)

$$M := \frac{V_1}{\sqrt{c_{s1}^2 + c_{A1}^2}} > 1 \quad . \quad (10.1.11)$$

M is called the *magnetoacoustic Mach number*. The sound velocity, c_s, and the Alfvén velocity, c_A, have been defined previously (Eqs. 3.2.12 and 3.2.13). Their combination in the denominator is the magnetoacoustic speed (Eq. 3.2.24). Equation (10.1.11) expresses that the shock must move faster than the magnetoacoustic speed in the upstream plasma. Condition (10.1.11) can be inverted to give $V_{x2} < \sqrt{(c_{s2}^2 + c_{A2}^2)}$. The physics of these conditions is that fast-mode disturbances in the downstream region reach the front and pile up; the front, however, cannot discharge into the region ahead. The strong shock jump relations (10.1.8 and 10.1.9) are valid for $M \gg 1$.

The ratio, β, of thermal to magnetic pressure (Eq. 3.1.51) controls the influence of the terms in Equation (10.1.10). For $\beta \ll 1$ – as in the solar corona – the magnetic pressure dominates, and the relevant Mach number is approximately the Alfvénic Mach number, $M \approx M_A := V_1/c_{A1}$.

Shocks propagating *parallel* to the magnetic field are particularly simple as the magnetic field terms drop out of the Rankine-Hugoniot relation (10.1.10). The jump conditions are purely hydrodynamic and identical to compression shocks of the sound mode. The shock condition (10.1.11) becomes $M = V_1/c_{s1} > 1$.

10.2. Collisionless Shocks in the Solar System

Cosmic shock theories were historically derived for hydrodynamic shocks in neutral gases. When the first evidence of shocks in the solar corona was identified in coronal radio type II bursts by R. Payne-Scott and coworkers in 1947, it was not clear that collisionless plasma waves were the source of the radio emission, nor was it known that they constitute an important part of the shock phenomenon. Soon after, T. Gold postulated shock waves propagating into interplanetary space and causing aurorae at Earth. Ten years later the IMP-1 satellite detected the bow shock of the Earth in the solar wind and opened a nearby testing ground for theories of collisionless shocks. Since then the fields of solar, interplanetary and planetary shocks have interacted fruitfully and are now growing together. Here we focus on fast-mode shocks, associated turbulent waves, and particle acceleration.

For all known shocks in the interplanetary medium, the population of accelerated particles carries relatively little mass, momentum, and energy, and therefore has a negligible impact on the large-scale dynamics. The macrostructure can be described approximately by single-fluid MHD equations (Section 10.1.2). Nevertheless, the single particle physics and collisionless processes – although of second order in the solar system – are important in astrophysics (in particular for cosmic ray acceleration). The kinetic microphysics has received great observational and theoretical attention for this reason. This overview of observations of shocks aims at a basic understanding of the most important kinetic processes.

10.2.1. Planetary and Cometary Bow Shocks

A collisionless shock forms as the super-Alfvénic solar wind hits a planet's magnetosphere. It is called *bow shock* in analogy to the non-linear waves forming at the bow of a boat moving faster than the surface gravity waves of water. The analogy should not be taken too literally since the wind flowing from the Sun carries the interplanetary magnetic field. This super-Alfvénic flow hitting an obstacle yields an illustrative example of a magnetic piston-driven shock. The kinetic shock phenomena are controlled by the magnetic field and strongly depend on the direction of the upstream field.

Figure 10.3 outlines the geometry of a bow shock for a planet with its own magnetic field. As qualitatively expected from MHD considerations (Section 10.1.1), the shock is much thinner where it is quasi-perpendicular (near A) than where it is quasi-parallel. Intense magnetic field fluctuations (indicated by wavy lines) are ubiquitous in the region ahead of the quasi-parallel shock. The various regions in the Earth's bow shock have been investigated extensively by orbiting satellites. Other spacecraft have flown through the bow shocks of nearly all other planets with similar results. Marked differences have only been found in bodies without magnetospheres (such as Venus, the Moon, and comets).

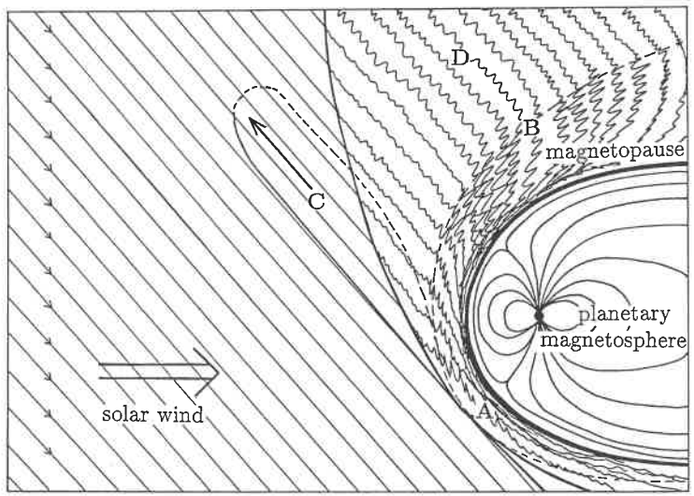

Fig. 10.3. A collisionless shock (dashed curve) forms as the solar wind impinges on the magnetosphere of a planet such as the Earth. The two plasmas and magnetic fields are separated by the magnetopause (thick curve). The points A and B mark the locations where the magnetic field relative to the shock normal is perpendicular and parallel, respectively. The magnetic field is compressed and variable in the shock. Energetic electrons and electron driven waves are observed in the electron foreshock C. Accelerated ions are unstable to magnetoacoustic waves forming the foot of the shock (or 'ion foreshock') D.

A. *Non-Thermal Particles*

Typically, 1% of the solar wind energy impinging on the Earth's magnetosphere is transferred to super-thermal particles in the upstream region. Most of the energy is taken up by ions. There are several particle populations distinct by energy and angular distributions.

- The population of reflected ions is most important: they form a steady field-aligned beam in the sunward direction with a velocity of about $-V_1$ in the frame of the shock (or a few keV). The ions are found on interplanetary field lines that are nearly tangent to the shock surface and connected to the bow shock at point A in Figure 10.3. (In other words, they are a result of the quasi-perpendicular shock.)

- An ion population having a broad energy distribution (with energies beyond 100 keV) is also observed. It is nearly isotropic and highly variable in density. These *diffuse ions* may (at least partially) originate from the above ion beam by quasi-linear diffusion (Section 7.3.3). Their energy density is comparable to that of the reflected ions. As an alternative, the theory of acceleration by quasi-parallel shock processes has also received wide support. The diffuse ions are observed downstream (anti-Sunward) of the reflected ions (in the upper right corner of Fig. 10.3), almost filling the entire ion foreshock region. In terms of total energy, they are the dominant non-thermal particle population.

- *Electron beams* of $1 - 2$ keV per particle are observed mainly on interplanetary magnetic field lines that are newly connected to the bow shock (electron foreshock, region C in Fig. 10.3). These field lines are nearly tangential to the shock front (point A in Fig. 10.3). Presumably, the electrons are accelerated where the field lines meet the shock in the quasi-perpendicular region. Because the particle velocities for these energies are much higher than the solar wind speed, energetic electrons can be found far upstream.

- The background electron distribution has a *super-thermal tail* in the sunward direction between the shock and the tangential field line.

- Electrons and protons with energies > 100 keV have been reported. They may also be a part of the electron beam and the diffusive ion populations, respectively. Compared to the other non-thermal particles, they are energetically unimportant.

B. *Upstream Waves*

The various non-thermal particle populations in the upstream region represent sources of free energy. They can drive many types of waves. The relation between observed waves and driving particles is not always clear.

Figure 10.4 displays the waves measured by a spacecraft traversing the Earth's bow shock from the solar wind (upstream) into the magnetosheath (region between shock front and magnetopause, cf. Fig. 10.3). The ordinate axis is observing time. The satellite moves at 83 km per minute. The amplitude of the oscillating electric and magnetic fields are shown in many channels at a large range of frequencies (top and middle). The magnetic field (given in Fig. 10.4, bottom) jumps by a factor of 3 from upstream to downstream. In the shock region, the overshoot even reaches 4.8 times the upstream value.

Most energetic in the absolute scale are large amplitude, low-frequency waves of the *fast magnetoacoustic* type (i.e. combining magnetic and density compressions like the MHD mode derived in Section 3.2.3). They are most prominent in the shock and downstream regions of Figure 10.4. Nevertheless, they also dominate energetically in the upstream plasma. As the waves are strongly correlated in time and space with the diffusive ions, the ions seem to be the source of the waves. An attractive possibility is the electromagnetic instability of ion beams (Section 7.3.1). As the solar wind moves faster than these waves, the waves are convected into the shock front and influence its nature. Also prominent (see Figure 10.4) but much weaker, are *whistler* waves, which may have several sources, including streaming ions and transverse electrons (Section 8.2.1).

Electron plasma waves near the plasma frequency are detected throughout the foreshock region. Their source is at the boundary of the electron foreshock. The waves correlate with the electron beams and have phase velocities of $1 - 2 \cdot 10^9$

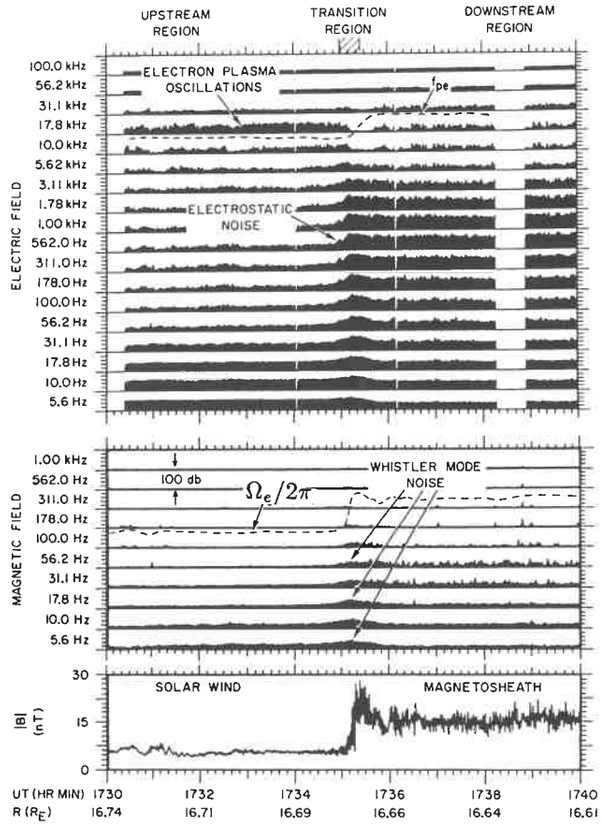

Fig. 10.4. The Earth's bow shock excites many wave modes. The wave electric (*top*) and magnetic (*middle*) fields are shown versus time as the ISEE–1 satellite traverses from the upstream into the downstream regions. The distance R from Earth center is also given in units of Earth radii. The spacing between frequencies is logarithmic. The plasma frequency and gyrofrequency are indicated by dashed curves. The amplitude scale is also logarithmic in each channel, ranging from the background to a factor of 10^{10} (100 dB). The background (DC) magnetic field strength is presented in the bottom panel in units of nanotesla ($= 10^{-5}$G). (After D.A. Gurnett, published in Tsurutani and Stone (eds.), 1985.)

cm s^{-1} corresponding to the observed electron energies of a few keV. A likely mechanism is the bump-on-tail instability (Section 5.2.4). In addition, *ion acoustic* waves, caused apparently by the diffusive ions, are frequently observed in the range 0.1−10 kHz (Fig. 10.4, labelled 'electrostatic noise'), upstream of the quasi-parallel shock region. At even lower frequencies ($\lesssim 50$ Hz), Figure 10.4 shows unidentified broadband and impulsive electrostatic emissions. In observations near the quasi-

perpendicular shock region, *lower hybrid* waves have been identified. They may be driven by reflected ions.

Distant spacecraft in the upstream solar wind have observed propagating *electromagnetic radiation* originating from the bow shock. Both the fundamental (at about the plasma frequency) and the harmonic emission have been detected. The bandwidth of the harmonic is very narrow, sometimes less than 3% of the center frequency. Two emission mechanisms have been proposed: (*i*) Langmuir waves may be driven unstable by the electron beams accelerated by the quasi-perpendicular shock. They could generate radio emission much like a solar type III burst (Section 6.3). (*ii*) Alternatively, a likely electron acceleration mechanism (to be discussed in Section 10.3.1) produces a loss-cone distribution. As in the solar wind $\omega_p/\Omega_e \approx 40$, the theory presented in Section 8.2 predicts instability for z-mode and upper hybrid waves (Eq. 8.2.23). The coupling of such waves, or an upper hybrid wave with a low-frequency wave then could produce radio emissions as in solar type IV bursts (Section 8.4.2), but from a small, narrowband source.

Finally, *Alfvén waves* have been discovered far upstream of bow shocks. They play a particularly prominent role in the shocks forming ahead of comets. As cometary nuclei are small and have a negligible magnetic field, comets generate shocks in a different way than planets. Sunlight evaporates atoms and molecules from the comet's surface, and solar UV radiation ionizes them. A plasma forms (called ionosphere), that cannot be penetrated by the solar wind (property of frozen in flux, Section 3.1.3). A few neutral atoms escape beyond the shock front between the cometary ionosphere and the solar wind. Ultimately ionized, they form a counter-streaming ion beam in the solar wind. Such a beam is prone to the classic electromagnetic ion beam instability of Alfvén waves (Section 7.3).

10.2.2. Interplanetary shocks

Interplanetary space is furrowed by shocks, in particular at distances beyond 1 AU from the Sun. Here we concentrate on the most abundant shocks, the fast-mode shocks produced by coronal mass ejections (CME). CMEs are observed by white-light coronagraphs and will be discussed in the next section.

The phenomena found in interplanetary travelling shocks are similar to the bow shocks ahead of planets. Not every interplanetary shock has all the bow shock features, however. The bow shocks comprise quasi-perpendicular as well as quasi-parallel sections; interplanetary shocks may have smaller curvature with less variation in shock angle. Generally, the density of non-thermal particles accelerated by interplanetary shocks is smaller, but the particles reach higher energy. Interplanetary shocks generally have a lower Mach number and a much greater spatial extent.

Interplanetary shocks are usually supercritical. They reflect and accelerate ions. The number of accelerated ions increases with Mach number; for quasi-parallel shocks, it was found to increase also with the upstream wave level. These relations are suggestive of first-order Fermi acceleration to be discussed in Section 10.3.2 (scattering between converging waves or shocks). Quasi-parallel shocks

cause non-thermal ions and ion acoustic turbulence millions of kilometers upstream.

Radio emissions are of particular interest as they yield information by remote sensing. Interplanetary shocks with detectable radio emission belong to the most energetic shocks produced by the Sun. They are associated with powerful flares and with the most massive and energetic CMEs. The radio emission decreases with distance from the Sun and usually disappears before about 0.7 AU in the background noise. Some shock-associated radio emission is produced by electron beams escaping far into the upstream region. Other emissions seem to originate near the shock. All radio sources, however, are located ahead of the interplanetary shock.

10.2.3. Coronal shocks

In the corona we can study much more powerful shocks, in which certain features are more pronounced. The radio emission alone (energetically a very minor phenomenon) emitted by a strong coronal shock sometimes exceeds the energy flux of all non-thermal particles upstream of the Earth's bow shock. Coronal shocks are also optically observable in Thomson scattered white light and by their footprints in the chromosphere (Moreton wave). Optical images give a global view of the phenomenon (Fig. 10.5), complementary to spacecraft observations probing the details along their trajectory.

A. *Coronal Mass Ejections*

Thomson scattering of electromagnetic radiation on free electrons is proportional to electron density. Density enhancements in the corona can be observed by coronagraphs (optical telescopes with an occulting device blocking the direct sunlight from the photosphere). Figure 10.5 shows material ejected by a coronal process. It produces a density enhancement that is observable on its way through the upper corona into interplanetary space. Such an event is called *coronal mass ejection* (CME).

In periods of high solar activity, more than one CME per day on average is observable with current techniques. They are related to eruptive prominences (also visible in Fig. 10.5) or flares. The speed of the leading edge ranges from less than 100 km s^{-1} to well beyond 1000 km s^{-1} at an estimated Alfvén velocity of 400 km s^{-1}. Apparently, not all CMEs are fast enough to be shocks. The flare-associated CMEs have generally a higher speed, and the fastest ones often propagate as far as 1 AU to be registered by spacecraft.

Curiously, detailed investigations have revealed that the relation between flare associated CMEs and flares are not as straightforward as one may think. CMEs can start up to 30 minutes before the flare. Thus the flare cannot be directly responsible for driving the CME. The CME seems to have its own driver that, under certain conditions, triggers a flare. CMEs are far more numerous than

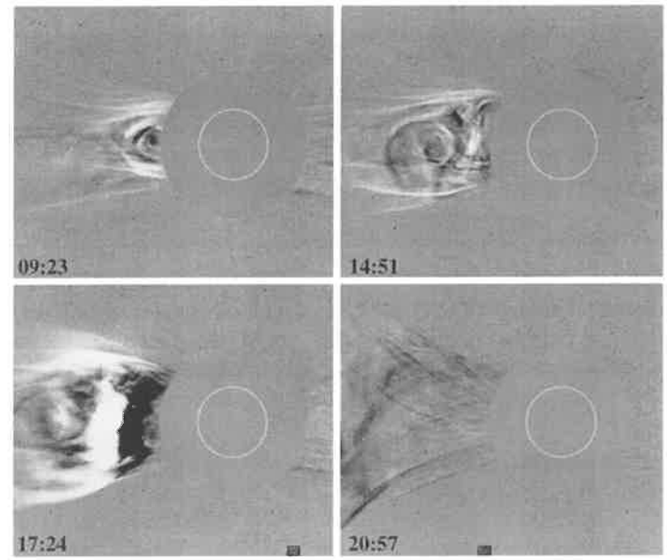

Fig. 10.5. The white light image of a coronal mass ejection (observed by the LASCO C2 coronagraph on the SoHO satellite) shows a bright arc moving out. The images are running differences to the preceding image. The white circle is the size of the photospheric disk (from Dere et al, 1999).

interplanetary shocks. For further details and references, the reader is referred to the reviews by Kahler (1987) and Hundhausen (1988).

B. *Type II Radio Bursts*

Extremely intense, narrow bands of radio emission caught the attention of the earliest observers. The bands are at harmonic frequencies having a ratio of slightly less than 1 : 2 and usually drift to lower frequency. The drift rate is typically two orders of magnitude smaller than for type III bursts produced by electron beams. The phenomenon has been named type II burst.

As an example, Figure 10.6 shows the start of a type II burst. After an interruption at 14:24:40, the event continues for more than 15 minutes. The observational characteristics are summarized in the following paragraphs. The references are listed in the reviews given at the end of the chapter.

The emission in two harmonic frequency bands is similar to the Earth's bow shock and to interplanetary shocks. It is suggestive of plasma emission near the plasma frequency and twice its value. The solar rate of frequency drift, combined with a density model, suggests radial velocities between 200 and 2000 km s^{-1}, about 2 orders of magnitude lower than type III bursts. Such outward source motions have been confirmed by multi-frequency radioheliographs. The enlargements

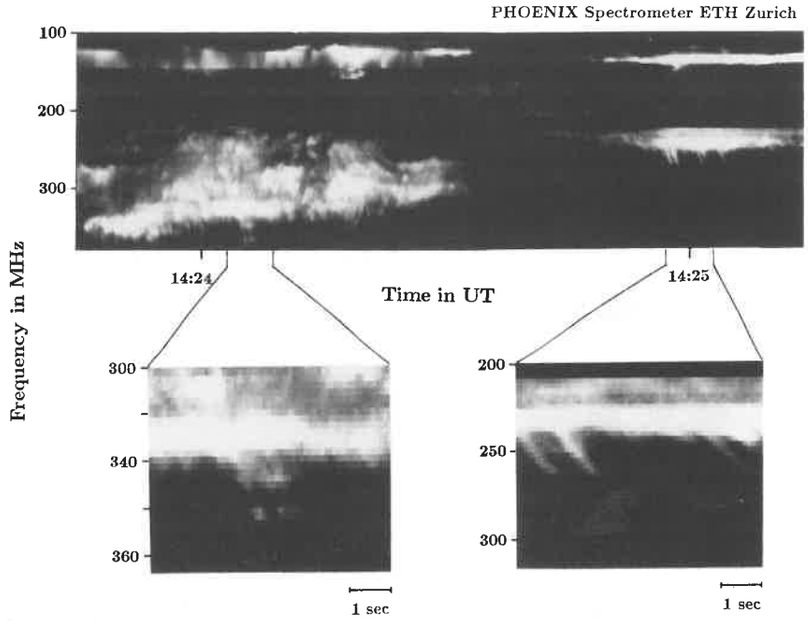

Fig. 10.6. Spectrogram of a section of a solar type II radio burst. The bright features indicate enhanced radio flux in logarithmic scale. *Bottom*: Two enlargements of the above overview showing horizontal 'backbone' and skew 'herringbone' emissions (from Benz and Thejappa, 1988).

in Figure 10.6 demonstrate that the radio emission has two components. A variable, narrow band drifts slowly to lower frequency at the same rate as the whole phenomenon. It is metaphorically termed the *backbone*. In addition, rapidly drifting, broadband structures shoot out of the backbone to higher and (not visible in Fig. 10.6) lower frequency. They are called *herringbones*. The two components are obviously different in their intrinsic time scale and bandwidth. Note that the backbone has a bandwidth of only $2-3\%$ at some time. If interpreted in terms of plasma emission ($\omega \approx \omega_p$), the bandwidth requires a source density homogeneity better than 5%, suggesting a small, stationary source moving with the shock. The herringbones resemble type III bursts and are generally interpreted as signatures of a beam of energetic electrons accelerated near the source of the backbone and escaping upstream from the shock. It is very likely that the herringbone emission is due to electron plasma waves excited by the bump-on-tail instability (Section 5.2.4) and scattered into radio waves by means similar to type III bursts.

Herringbone emission, and thus appreciable electron acceleration, occurs only in about 20% of all type II bursts. The stronger the backbone emission, the more likely are herringbones. The backbone flux density correlates with shock velocity (e.g. Cane and White, 1989).

Only 65% of the shocks observed as a fast ($v > 500$ km s^{-1}) coronal mass ejection radiate type II emission. On the other hand, CMEs slower than 200 km s^{-1} are occasionally accompanied by type II bursts (e.g. Kahler *et al.*, 1985). Furthermore, type II bursts often end around 20 MHz (about 2 $R_\odot$ from the center of the Sun) while the shocks apparently continue. There seem to be additional conditions on electron acceleration and radio emission.

Type II associated shocks are generally productive in particle acceleration, manifest in significant associations with interplanetary proton streams and coronal type IV radio emission. The causal relation to flares is clear for type II bursts. They start about one minute after the peak of the flare hard X-rays and are more delayed the lower the starting frequency.

A tentative and popular scenario proposes CME to be flare independent shocks, piston-driven by rising magnetic loops. If a large flare is associated, the flare blast wave – starting later and catching up from behind – causes a type II-emitting, high Mach number shock. A blast wave interpretation is attractive due to the property of all waves (including shocks) to refract toward regions of low phase velocity (see for example Fig. 6.4). As the energy of a shock is approximately conserved, the magnetoacoustic Mach number increases in such a region. For the same reason, the shock would develop into a more quasi-perpendicular type, prone to electron acceleration (Section 10.3.1). This scenario is awaiting observational confirmation.

10.3. Particle Acceleration and Heating by Shocks

Particle acceleration is a characteristic property of collisionless shocks. There are two types of acceleration processes. (*i*) Most important are mechanisms reflecting upstream particles by the moving front. There are several derivatives of this idea, two will be presented in Sections 10.3.1 (for electrons) and 10.3.2 (for ions). (*ii*) In addition, the upstream wave turbulence can heat or – more generally – energize background particles (primarily electrons). It will be discussed in Section 10.3.3. These types of acceleration should not be considered a complete list of all possible acceleration processes at shocks.

10.3.1. Electron Acceleration at Quasi-Perpendicular Shocks

In 1949 E. Fermi proposed that 'magnetic clouds' moving in the Galaxy could accelerate charged particles to cosmic ray energies. He did not use the word 'shock', but considered magnetic mirrors (Section 2.1.2) embedded in the clouds that elastically reflect particles. In the observer's frame of reference, the particle gains energy in a head-on collision (opposite initial velocities of particle and mirror), and it loses energy in a catch-up collision, when the particle approaches the mirror from behind.

Fermi later developed the idea into two types of acceleration mechanisms. In the *first-order* Fermi process, two mirrors approach each other and the particles in between collide many times, gaining energy at each reflection. The *second*

type assumes clouds moving in random directions. Since head-on collisions are statistically more likely than catch-up ones, the colliding particles gain energy on the average. Both historic concepts are still in use, although modified in details. The first-order Fermi process, being simpler to realize and more efficient, will be studied first.

In this section we concentrate on a single reflection with high shock velocity. The process is referred to as *shock drift acceleration* or fast-Fermi acceleration. Assume that the gyroradius of a charged particle is much smaller than the shock thickness. Then a shock can act like a magnetic mirror, as there is an increase in magnetic field strength across the front for fast-mode shocks (Eqs. 10.1.2 – 10.1.7). The magnetic moment of the particle is conserved in the shock-particle interaction. According to Equation (2.2.3) and if there were no electric field, a particle with velocity v is reflected under the condition

$$B_m > B_1 \left(\frac{v}{v_\perp^1} \right)^2 \quad , \tag{10.3.1}$$

where the superscript 1 refers to the values before the encounter, and B_m is the mirroring magnetic field in the shock front. However, Equation (10.3.1) is not generally valid, since $\mathbf{E}$ is usually not zero – neither in the observer's frame nor the normal incidence frame defined in Section 10.1 – as $\mathbf{E} = -(\mathbf{V} \times \mathbf{B})/c$. For this reason, we have to study a special frame of reference in the following subsection, where Equation (10.3.1) can be used.

A. *De Hoffmann-Teller Frame*

Equation (10.3.1) only holds in the particular reference frame where the electric field due to the upstream plasma motion vanishes. This is known as the *de Hoffmann-Teller (HT) frame*, in reference to early workers in collisionless shock theory. In this frame the shock front is at rest and the upstream flow is along the magnetic field, thus $\mathbf{V}_1^{\mathrm{HT}} \times \mathbf{B}_1 = 0$. The HT frame moves along the shock front relative to the normal incidence frame with a velocity V_{HT} so that in the HT frame one would see the upstream plasma flowing in along the magnetic field lines. This is the geometry of somebody watching rain from a moving car. The speed, V_{HT}, is chosen to see the flow coming at the given angle θ_1 from zenith, where θ_1 is the magnetic field angle to the shock normal, $\mathbf{n}$ (Fig. 10.7), namely

$$\mathbf{V}_{\mathrm{HT}} = \frac{\mathbf{n} \times (\mathbf{V}_1 \times \mathbf{B}_1)}{\mathbf{B}_1 \cdot \mathbf{n}} = V_1 \tan\theta_1 \quad . \tag{10.3.2}$$

As observed in the normal incidence frame, $\mathbf{V}_{\mathrm{HT}}$ is simply the velocity at which the intersection point of a given field line and the shock surface moves along the shock front. Faraday's law requires the flow behind the shock to be also aligned with the magnetic field in the HT frame.

The upstream inflow velocity in the HT frame, V_1^{HT} (not to be confused with V_{HT}, see Fig. 10.7), is along the magnetic field by definition. It amounts to

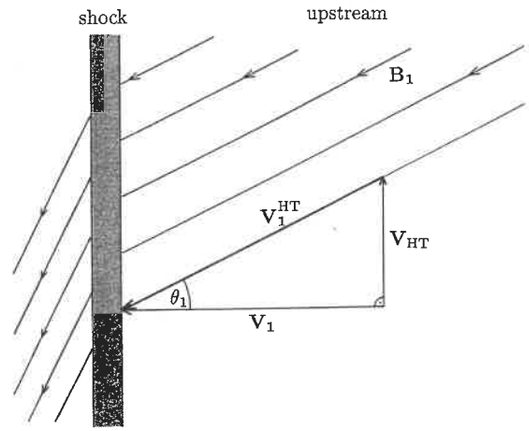

Fig. 10.7. Upstream flow velocities in the normal incidence frame of reference, $\mathbf{V}_1$, and in the de Hoffmann-Teller frame, $\mathbf{V}_1^{\mathrm{HT}}$. The transformation velocity, $\mathbf{V}_{\mathrm{HT}}$, is parallel to the shock front.

$$V_1^{\mathrm{HT}} = \frac{V_1}{\cos\theta_1} \tag{10.3.3}$$

from simple geometry. In the HT frame, the upstream flow of a quasi-perpendicular shock hits the front at a high velocity as $\cos\theta_1 \ll 1$. In the observer's frame, where the intersection with the shock moves along a given field line at a high velocity, one anticipates that the reflected particles gain considerable energy. We shall investigate this in the following section.

B. *Electron Acceleration*

Since there is no electric field, the magnetic moment of a charged particle is conserved in the HT frame of reference. According to Equation (10.3.1), particles with a pitch angle $\alpha > \alpha_c := \arcsin(B_1/B_2)^{1/2}$ – i.e. those with high transverse velocities – are reflected. Figure 10.8, drawn in the HT frame, displays the velocity distribution. Incoming particles are found at an average parallel velocity of $-V_1^{\mathrm{HT}}$, and reflected particles are shifted to $+V_1^{\mathrm{HT}}$. Reflection is limited to particles with large pitch angle in the HT frame. As the condition for reflection (Eq. 10.3.1) is independent of charge and mass, and as electrons have a much faster transverse motion, there are more electrons reflected than ions. Shocks with high inflow speed accelerate electrons to the highest energies and will be of primary interest. If V_1^{HT} is large – that is, in nearly perpendicular shocks – reflection is limited to the electrons with the largest pitch angle (i.e. to a fraction of the halo population in Fig. 10.8).

We have neglected any electric fields in the shock layer building up by preferential electron acceleration or by local field fluctuations. They can be included easily into the orbit calculation through a potential. Its effect is to further reduce the population of reflected electrons particularly at low parallel velocity.

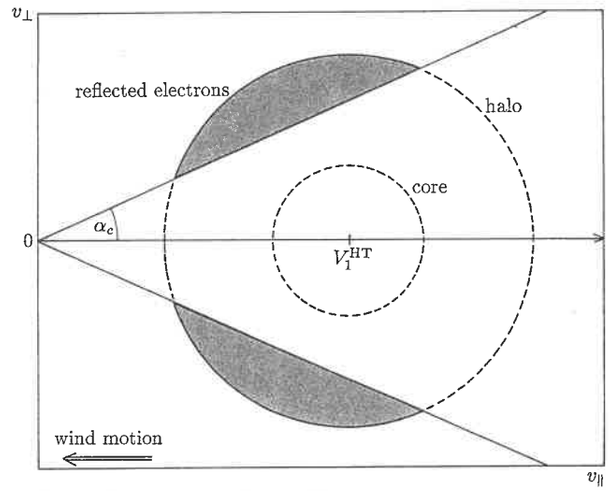

Fig. 10.8. Schematic velocity distribution of upstream electrons in the de Hoffmann-Teller frame of reference. The reflected electrons are shaded. The coordinates are chosen parallel (sunward is positive) and perpendicular to the magnetic field. The initial distribution is assumed to have two Maxwellian populations forming a core and a halo. The halo corresponds to a tail in the upstream velocity distribution providing the seed particles for acceleration.

In the HT frame, the particles are reflected at the same energy, but negative velocity. The Lorentz transformation by $\mathbf{V}_1^{HT}$ into the normal incidence frame, reveals that the reflected particles gain energy. A particle with a velocity $v_\parallel^{HT}$ parallel to the magnetic field in the HT frame has a larger velocity in the normal incidence frame (ni) by the transformation velocity. The y-component (Fig. 10.2) is of primary interest and is given by

$$v_y^{ni} = \frac{v_\parallel^{HT} \sin\theta_1 + V_{HT}}{1 + v_\parallel^{HT} \sin\theta_1 V_{HT}/c^2} \quad . \tag{10.3.4}$$

The denominator in Equation (10.3.4) is required by the theorem of velocity addition in special relativity. For nearly perpendicular shocks ($V_{HT} \gg v_\parallel^{HT}$), the particles are reflected with about V_{HT}, which was given by Equation (10.3.2) and is limited by the speed of light.

The distribution of reflected particles (Fig. 10.8) may be called a displaced loss-cone. It resembles the distributions of trapped particles in its inverted distribution of transverse energy. Additionally, it has the properties of a stream. The two positive gradients in velocity space – in perpendicular as well as parallel directions – drive instabilities similar to trapped particles and beams. In an initial phase, still close to the shock, the distribution will relax to a plateau-like distribution, releasing its transverse free energy and a part of its parallel free energy. This process may be the source of the radiation seen in the backbone of solar type II radio bursts (Section 10.2.3). The plateau-distribution propagates subsequently away from the shock, producing electrostatic plasma waves at its front. It is very likely the source of the herringbones in type II bursts.

Drift (or fast-Fermi) acceleration can explain the observed energetic electrons at the Earth's bow shock. It is likely to take place in the solar corona and possibly in supernova remnants. Furthermore, the process is also proposed to accelerate intermittent ion beams observed from the quasi-perpendicular region of the Earth's bow shock.

10.3.2. Ion Acceleration at Quasi-Parallel Shocks

Shock drift acceleration discussed in the previous section is primarily effective for a halo electron population. Now we study an acceleration process that is well suited for ions. If some ions are reflected on a shock front, they carry much free energy into the upstream region and can drive low-frequency, electromagnetic beam instabilities according to Section 7.3. Strong magnetoacoustic and Alfvén waves have been observed and interpreted this way. As the ions excite waves, they diffuse in velocity space into a more isotropic distribution (Section 6.2.1). The average ion velocity is drastically reduced. Since the shock speed exceeds the magnetoacoustic velocity, the inflow drives eventually the ions – trapped in their self-excited waves – back to the shock front. The particles experience repeated reflections between the waves and the front. The process is known as *diffusive shock acceleration*. It is important to note that the particles are not accelerated in a single step, but by multiple scatterings off a single shock. The upstream waves are overtaken by the shock, both together provide for a set of converging mirrors, characteristic for first-order Fermi acceleration. If electrons and ions get accelerated to similar velocities, the ions gain more energy due to their larger mass.

Diffusive acceleration can be modelled in a simple way, following the approach of Bell (1978). Let χ be the ratio of particle energy increase per reflection in the observer's frame. In a one-dimensional geometry (head-on collisions only), a particle with an initial velocity v_i reflected by a shock having a velocity in the observer's frame of $V_1^{obs} \ll v_i$ gains kinetic energy by a factor of

$$\chi := \frac{\varepsilon + \Delta\varepsilon}{\varepsilon} \approx 1 + 4\frac{V_1^{obs}}{v_i} \quad . \tag{10.3.5}$$

Equation (10.3.5) is non-relativistic. The relativistic energy gain is calculated from energy and momentum conservation in the HT frame. Without loss of generality, we assume one spatial dimension and Lorentz transform to the observer's frame. One finds that the particle energy changes in the observer's frame by

$$\Delta\varepsilon = 2\varepsilon_i\gamma_1^2\frac{V_1^{obs}(v_i + V_1^{obs})}{c^2} \quad , \tag{10.3.6}$$

where ε_i is the total initial energy, $m\gamma_i c^2$, and γ_1 is the Lorentz factor of the shock velocity, both in the observer's frame (Exercise 10.5). The energy gain is reduced

by a factor of 2 when averaged over angles in three dimensions. For $v_i \approx c$, and $V_1^{\rm obs} \ll c$ (thus $\gamma_1 \approx 1$),

$$\chi \approx 1 + \frac{V_1^{\rm obs}}{c} \quad . \tag{10.3.7}$$

Furthermore, let P be the probability that the particle remains in the upstream region and will have another reflection ($P \leq 1$). Let us start with a density n_0 of particles with an initial energy ε_0. After j reflections there is a density of $n = n_0 P^j$ particles with energies $\varepsilon = \varepsilon_0 \chi^j$. After taking the logarithm and eliminating j, the two relations combine to

$$n(\geq \varepsilon) = n_0 \left(\frac{\varepsilon}{\varepsilon_0} \right)^{\ln P / \ln \chi} \quad , \tag{10.3.8}$$

a power-law distribution. As n refers to the particles that have reached the energy ε and are further accelerated, it is related to the spectral energy density by $n(\geq \varepsilon) = \int_\varepsilon^\infty f(\varepsilon) d\varepsilon$. The energy distribution, $f(\varepsilon)$, is the derivative of Equation (10.3.8). It is also a power law of the form $f(\varepsilon) \propto \varepsilon^{-\delta}$, where δ is the power-law index of the energy distribution, amounting to

$$\delta = 1 - \frac{\ln P}{\ln \chi} \quad . \tag{10.3.9}$$

There are several approaches to estimate P, the fraction of particles of an isotropic distribution that is reflected. In the simplest version, often used for cosmic rays, it is assumed that the shock front is completely permeable to energetic ions from both sides. The ions ($v \approx c$ and trapped in magnetic field fluctuations) have the same density n on both sides and move through the front at a rate of $nc/4$. Let us assume that particles are only lost by convecting away in the downstream region. The loss rate then is nV_2 or about $nV_1/4$ in the strong shock limit (Eq. 10.1.8). The probability of escape is V_1/c, thus $P \approx 1 - V_1/c$ and $\delta \approx 2$. This value becomes larger if the average compression factor (Eq. 10.1.8) is below 4, as often observed at the bow shock. The predicted power-law exponent thus is close to the one observed in the cosmic ray spectrum (Section 7.1.2).

10.3.3. Resonant Acceleration and Heating

The entropy jumps in the plasma flowing through the shock front. Thus the temperature increases non-reversibly. In collisionless shocks, microscopic electric and magnetic fields are the source of the entropy increase. The interaction of particles with these field fluctuations drains energy from the shock and heats the plasma.

An example is heating of electrons by magnetic compression. It is an intrinsically adiabatic process, but can be made irreversible by wave turbulence. If the shock thickness is larger than the gyroradius, particles penetrating the shock conserve their magnetic moment. Equation (2.1.7) in relativistic form reads as

$$\frac{(p_\perp^1)^2}{B_1} = \frac{(p_\perp^2)^2}{B_2} \quad , \tag{10.3.10}$$

where $p_\perp = \gamma m v_\perp$ is the perpendicular particle momentum, and the superscripts 1 and 2 refer to the upstream and downstream plasma, respectively. The process is also known as *betatron acceleration* in analogy to the laboratory application. The maximum increase of the magnetic field predicted by MHD theory (Eq. 10.1.10) for strong perpendicular shocks is $B_2/B_1 = 4$. The magnetic field in the Earth's bow shock is often observed to overshoot four times the upstream value (Fig. 10.4). Nevertheless, very high energies cannot be achieved through this simple version of the betatron process. Even worse, in a subsequent expansion of the magnetic field the particle loses all the energy gain since the process is reversible.

A betatron-accelerated population is anisotropic in velocity space because the particles gain only transverse energy. If pitch angles are isotropized in a random way before expansion, some heating is irreversible. The cycle may repeat many times. In each cycle, the particles experience a net energy gain. This process has been called *magnetic pumping*.

Magnetic pumping could be particularly effective in the strong low-frequency turbulence ahead of quasi-parallel shocks (ion foreshock) where the waves take the role of magnetic pumps. It has been proposed that electrons could be accelerated this way and be subsequently scattered in pitch angle by whistler waves.

Another form of heating is *resonance acceleration*. An example has already been given in Section 9.4.3 on particle acceleration by currents. The essence of the mechanism is wave turbulence created by one particle population that stochastically accelerates another population. The process is a diffusion in velocity space. As pointed out in Section 9.4.3, lower hybrid waves are an attractive medium to transfer energy from ions to electrons. Perpendicular currents in the form of moving ions exist in oblique shock fronts. Perpendicular ion flows are unstable toward growing lower hybrid waves. The scenario is supported by observations at the Earth's bow shock, where lower hybrid waves have been discovered that may occasionally accelerate electrons in parallel velocity.

10.4. Stochastic Particle Acceleration

Concerning Fermi acceleration on magnetic mirros we have so far considered only first-order models. These processes, however, are not consistent with observations of the prompt acceleration of electrons and ions in flares, where acceleration of large numbers of particles is required preceding the observed shocks in the high corona and interplanetary space. Second-order Fermi acceleration is most attractive where shocks or large amplitude waves propagate in a limited volume such as the reconnection outflows and energize some or most of its particles. Charged particles move along magnetic field lines and thus get accelerated in the direction parallel to the magnetic field in head-on collisions. The particles lose energy in the

slightly less frequent catch-up encounters. Thus their energy varies stochastically in both directions, but has a trend to increase.

If waves act as the mirrors, only a small fraction of the particles is affected. The interaction requires a resonance condition of the type

$$\omega - k_z v_z = l\Omega_\alpha \quad . \tag{10.4.1}$$

Contrary to (non-resonant) Fermi acceleration, a spectrum of waves is now necessary for substantial acceleration. A particle having gained energy then can interact with another wave meeting its new resonance condition for further energy gain. Attractive for particle acceleration are waves that resonate with particles in the bulk part of the thermal velocity distribution. Such waves can act as primary accelerators without needing already fast seed particles. In addition, waves are required that are naturally formed in a situation of magnetic reconnection.

Of particular interest for flare electron acceleration are oblique fast magnetoacoustic waves (also called compressional Alfvén waves, see Section 3.2.4). These waves have a dispersion relation $\omega \approx kc_A$ (assuming $c_A \gg c_s$) from the MHD range up to about the proton gyrofrequency. Above about $10\Omega_p$, the branch enters the whistler regime having enhanced phase velocity. As $c_A < v_{te}$, the waves are in $l = 0$ (Čerenkov) resonance with the bulk part of the thermal electrons, but generally not with the ions.

Fast magnetoacoustic waves have an oscillating wave magnetic field component parallel to the undisturbed field. It produces a series of compressive and rarefactive perturbations moving in parallel direction with a velocity of about $v_A/\cos\theta$, where θ is the angle between $\mathbf{k}$ and B_0. If the distribution of waves is isotropic, the range of phase velocity projections in z-direction is continuous from v_A to infinity.

This characteristic property makes it easy to envisage the interaction with electrons. The oscillations act as magnetic mirrors for charged particles like converging fields (Section 2.2). If the gyroradius is much smaller than the scale of contraction, the particles experience a mirror force $-\mu\partial B_z/\partial z$ (Eq. 2.1.12), and those with pitch angles above a critical value are reflected. The critical value depends on the wave amplitude. In small amplitude waves, only particles moving nearly in phase with the wave are reflected. Then the resonance condition (10.4.1) must be closely satisfied. In the frame moving with the wave, reflected particles have large pitch angles as the loss-cone is nearly 90°. For larger amplitudes, the velocity range of interaction becomes larger and more particles interact. In reality, the waves should not be envisaged as infinite sinusoidals, but distributions in frequency, angle, and amplitude of finite wave packets. Then it becomes easy to conceptualize a transition to (non-resonant) shocks.

If more interacting particles are slightly slower than the parallel wave phase velocity, the particles gain on the average and the wave is damped by the interaction. It is thus the magnetic analog to Landau damping of a wave with parallel electric field (Section 5.2.3). The resonance condition (Eq. 10.4.1, with $l = 0$) can be rewritten as $\lambda_z/v_z \approx \tau$, where τ is the wave period and $\lambda_z = 2\pi/k\cos\theta$ is the parallel wavelength. A small amplitude wave and a particle interact if the particle transit time across the wavelength is approximately equal to the period.

This property is the origin of the name *transit-time damping* for this acceleration process. It is basically resonant second-order Fermi acceleration.

Electron acceleration by transit-time damping has a major drawback. The acceleration is in parallel direction only. As v_z increases, the pitch angle $\alpha = \arctan(v_\perp/v_z)$ therefore decreases. The requirement on the wave amplitude for reflection increases until it cannot be satisfied anymore and acceleration stops. Several processes have been proposed that may scatter the accelerated electrons into more transverse orbits, such as collisions or a pre-existing population of whistler waves. Most likely, however, is that the velocity distribution stretches out into parallel direction until it becomes unstable to L-mode waves by anomalous Doppler resonance. This is named the *electron firehose instability*.

Fast magnetoacoustic waves may originate in the rearrangement of the large-scale magnetic field by reconnection jets or their shear flow instabilities. Long wavelength modes cascade to smaller wavelengths to reach eventually waves with a sufficiently high k_z to interact with thermal electrons, when they are transit-time damped. The electron acceleration process can then be described by quasi-linear diffusion (Section 6.2.1). If the pitch angle distribution remains more or less isotropic, electron acceleration by transit-time damping can proceed to ultrarelativistic velocities within a fraction of a second.

Large amplitude, fast magnetoacoustic waves preferentially accelerate electrons by the $l = 0$ resonance. The $l \neq 0$ resonances in Eq. (10.4.1)are negligible as long as the conditions for transit-time acceleration are satisfied. A similar scenario has also been proposed for flare proton acceleration, assuming Alfvén waves and $l \neq 0$ resonances. Stochastic acceleration is a simple and most promising process for flares if the required input wave turbulence is given.

Exercises

10.1: The thickness Δx of a shock front is given by the scale over which the inflowing energy can be dissipated. Do a thought experiment to study whether this may occur by Ohmic dissipation. An MHD shock is assumed to move in x-direction. B_{1y} and B_{2y} are the transverse field components ahead and behind the shock in the rest frame of the shock, respectively. For a strong shock, the magnetic field compression is $B_{2y} \approx 4B_{1y}$. The kinetic energy density deposited by the inflowing plasma in the shock layer is $\Delta\mathcal{E} \approx \frac{1}{2}\rho_1 V_1^2$. This must occur within a time $\Delta t \approx \Delta x/V_1$. Use Coulomb conductivity and, as an alternative, the minimum anomalous conductivity (Eq. 9.4.3); let $T = 10^6$ K, $c_A = 10^8$ cm s^{-1}, $M_A := V_1/c_A = 3$, and $n_e = 10^9$ cm^{-3}. Apply Equation (10.1.1) and

$$J \approx \frac{c}{4\pi} \frac{B_{1y} - B_{2y}}{\Delta x} \tag{10.4.2}$$

to calculate the shock thickness Δx.

10.2: For high Mach number shocks, the kinetic energy inflow largely exceeds the thermal energy and magnetic energy. The inflowing energy then is partitioned between kinetic, thermal, and magnetic energy density in the downstream medium. The division is independent of Mach number as stated by Equations (10.1.8) and (10.1.9). Prove these equations!

10.3: A gradient in magnetic field strength perpendicular to the field causes a gradient current. Calculate the scale length of the field in perpendicular direction required to cause a current drift velocity, V_d, equal to the ion sound velocity, c_{is}. Take for example $T_l = T_i = 10^7$ K, $n_e = 10^{10}$ cm^{-3}, $B = 100$ G.

10.4: A bow shock forms where the solar wind hits the magnetosphere of the Earth. Calculate the distance r of the plasma pause (the surface separating the two plasmas) from the center of the Earth in the direction toward the Sun. Use momentum conservation at the shock front and assume constant pressure between front and pause. Let the solar wind have a proton density of 5 cm^{-3}, magnetic field of $2 \cdot 10^{-4}$ G, temperature 10^5 K, and a velocity of 400 km s^{-1}, and assume a terrestrial magnetic field in the equatorial plane of $B(r) = 0.3(r/R_\oplus)^3$ G. Why does MHD give the correct answer?

10.5: A particle with initial velocity v_i and initial energy ε_i gains energy when reflected by a shock moving at $V_1^{\rm obs}$ in the observers frame of reference. Assume a head-on collision and a one-dimensional geometry. Energy ε and three-momentum $\mathbf{p}$ are Lorentz transformed into the frame moving with the shock, where

$$\varepsilon' = \gamma_1(\varepsilon + pV_1^{\rm obs}) \quad , \tag{10.4.3}$$

$$\mathbf{p}' = \gamma_1(\mathbf{p} + \frac{V_1^{\rm obs}\varepsilon}{c^2}) \quad , \tag{10.4.4}$$

where $\gamma_1 = (1 - (V_1^{\rm obs}/c)^2)^{-1/2}$ is the Lorentz factor of the shock. What is the energy gain per reflection? Prove Equations (10.3.5) and (10.3.6).

Further Reading and References

General reviews

Tidman, D.A. and Krall, N.A.: 1971, *Shock Waves in Collisionless Plasmas*, Wiley-Interscience, New York.

Tsurutani, B.T. and Stone, R.G. (eds.): 1985, 'Collisionless Shocks in the Heliosphere', *Geophysical Monograph* **35**, American Geophysical Union, Washington.

Priest, E.R.: 1982, *Solar Magnetohydrodynamics*, D. Reidel Publishing Comp., Dordrecht, Holland, Chapter 5 on MHD shocks.

Observations of shocks

Aurass, H.: 1992, 'Radio Observations of Coronal and Interplanetary Type II Bursts', *Am. Geophys.* **10**, 359.

Bavassano-Cattaneo, M.B., Tsurutani, B.T., and Smith, E.J.: 1986, 'Subcritical and Supercritical Interplanetary Shocks: Magnetic Field and Energetic Particle Observations', *J. Geophys. Res.* **91**, 11929.

Hundhausen, A.J.: 1988, 'The Origin and Propagation of Coronal Mass Ejections', *Proc. Sixth Int. Solar Wind Conf.* (V.J. Pizzo, T.E. Holzer, and D.G. Sime, eds.), NCAR Tech. Note, TN-**306**, Vol. 1, p. 181.

Kahler, S.W.: 1987, 'Coronal Mass Ejections', *Rev. Geophys.* **25**, 663.

Mann, G.: 1995, 'Theory and Observations of Coronal Shock Waves', in *Coronal Magnetic Energy Releases,* (A.O. Benz and A. Krüger, eds.), Lecture Notes in Physics **444**, 183.

Nelson, G.J. and Melrose, D.B.: 1985, in *Solar Radiophysics* (D.J. McLean and N.R. Labrum, eds.), Cambridge University Press, Chapter 13 on type II radio bursts.

Russel, C.T. and Hoppe, M.M.: 1983, 'Upstream Waves and Particles', *Space Science Rev.* **34**, 155.

Particle acceleration

Decker, R.B.: 1988, 'Computer Modelling of Test Particle Acceleration at Oblique Shocks', *Space Sci. Rev.* **48**, 195.

Jones, F.C. and Ellison, D.C.: 1991, 'The Plasma Physics of Shock Acceleration', *Space Sci. Rev.* **58**, 259.

Holman, G.D. and Pesses, M. E.: 1983, 'Solar Type II Radio Emission and the Shock Drift Acceleration of Electrons', *Astrophys. J.* **267**, 837.

Lee, M.A.: 1983, 'Coupled Hydromagnetic Wave Excitation and Ion Acceleration at Interplanetary Traveling Shocks', *J. Geophys. Res.* **88**, 6109.

Miller, J.A.: 1997, 'Electron Acceleration in Solar Flares by Fast Mode Waves: Quasi-linear Theory and Pitch-angle Scattering', *Astrophys. J.* **491**, 939.

Schlickeiser, R. and Steinacker, J.: 1989, 'Particle Acceleration in Impulsive Solar Flares II. Nonrelativistic Protons and Ions', *Solar Phys.* **122**, 29.

References

Bell, A.R.: 1978, 'The Acceleration of Cosmic Rays in Shock Fronts', MNRAS **182**, 147.

Benz, A.O. and Thejappa, G.: 1988, 'Radio Emission of Coronal Shock Waves', *Astron. Astrophys.* **202**, 267.

Cane, H.V. and White, S.M.: 1989, 'On the Source Conditions for Herringbone Structure in Type II Solar Radio Bursts', *Solar Phys.* **120**, 137.

Dere, K. P., Brueckner, G. E., Howard, R. A., Michels, D. J. and Delaboudiniere, J.: 1991, 'LASCO and EIT Observations of Helical Structure in Coronal Mass Ejections', *Astrophys. J.* **516**, 465.

Kahler, S.W., Reames, D.V., Sheeley, N.R.Jr., Howard, R.A., Koomen, M.J., and Michels, D.J.: 1985, 'A Comparison of Solar ^{3}Helium-Rich Events with Type II Bursts and Coronal Mass Ejections', *Astrophys. J.* **290**, 742.